Environmental Science: Atmospheres

ROYAL SOCIETY OF CHEMISTRY

PAPER

Published on 30 July 2026
Licensed under CC-BY 4.0

Check for updates

Cite this: *Environ. Sci.: Atmos.*, 2026, **6**, 1453

Nocturnal agricultural fires contribute to secondary brown carbon in the rural Po Valley

Julia David, *[a] Luca D'Angelo,[b] Asta Gregorič,[cd] Martin Rigler,[c] Vaios Moschos,[e] Luca Ferrero[f] and Alexander L. Vogel *[a]

Agricultural residue burning is a major source of biomass burning organic aerosol and organic reactive gases, contributing significantly to atmospheric brown carbon (BrC). The occurrence of agricultural fires, and the chemical evolution of their emissions toward BrC remains largely unknown. Here we show that frequent transient biomass burning events occur during autumn in rural Po Valley. We found that ~80% of detected organic compounds originate from nocturnal biomass burning, impacting air quality and radiative heating on the following day. Characterizing the molecular absorption properties of individual organic compounds using real-time Orbitrap mass spectrometry, we find a transient cluster containing species that peak during biomass burning events, while sustained clusters are dominated by a larger fraction of absorbing compounds. Simultaneous absorption measurements show that secondary BrC dominates BrC-induced radiative heating, contributing 71.0 ± 1.8% (0.031 ± 0.001 K day^{-1}) compared with primary BrC heating. Our results highlight the need to integrate secondary BrC formation into regional climate and air quality models, particularly in agricultural regions where nighttime burning strongly contribute to radiative aerosols formation. The findings suggest that stricter enforcement of European and regional bans on open-field burning represents an effective measure to improve regional air quality while reducing local radiative forcing.

Received 17th March 2026
Accepted 7th July 2026

DOI: 10.1039/d6ea00037a

rsc.li/esatmospheres

Environmental significance

Agricultural biomass burning is a widespread source of atmospheric pollutants and light-absorbing particles. By combining real-time high-resolution mass spectrometry with optical measurements, we provide new molecular level insights into biomass burning aerosol composition, its evolving light absorption and resulting atmospheric heating rates. These results improve the understanding of BrC composition and effects and indicate the need for stricter implementation of existing air quality regulations to mitigate both health and climate impacts from air pollution in agricultural regions.

Introduction

Light-absorbing organic aerosol, commonly referred to as brown carbon (BrC), absorbs solar radiation, influences atmospheric chemistry, and can contribute to atmospheric warming. Substantial amounts of particulate matter (PM) including BrC-containing organic aerosol (OA) are emitted from biomass burning (BB), which frequently occurs worldwide due to both natural and anthropogenic causes.[1,2] BB-derived OA (BBOA) includes both primary organic aerosol (POA) released directly, and secondary organic aerosol (SOA) formed through oxidation of BB volatile organic compounds (VOCs). Additionally to BrC, light-absorbing aerosol (LAA) includes black carbon (BC) and mineral dust from non-combustion sources, which, together with BrC, significantly affect atmospheric composition and climate through their optical and radiative properties. LAAs act as short-lived climate forcers with strong effects on Earth's radiation balance. Among these, BC is a strong climate forcer, ranking behind CO_2, CH_4 and N_2O, while BrC may account for 10–30% of total LAA solar absorption.[4–6]

Laboratory studies demonstrate that nitrate radical ($^{\bullet}NO_3$) oxidation of BBOA-formation proxies can form secondary BrC and substantially alter optical properties by forming new light-absorbing products, providing a mechanistic basis for nocturnal BrC enhancement.[7] Recent field observations show prominent nighttime formation of SOA with strong light absorption and a spectral dependence that differs from primary

[a]*Institute for Atmospheric and Environmental Sciences, Goethe University Frankfurt, 60438 Frankfurt am Main, Germany. E-mail: David@iau.uni-frankfurt.de; Vogel@iau.uni-frankfurt.de*

[b]*Environmental Protection Agency of Lombardy Region (ARPA Lombardia), Milano, 20124, Italy*

[c]*Aerosol d.o.o., Ljubljana, 1000, Slovenia*

[d]*Centre for Atmospheric Research, University of Nova Gorica, Ajdovščina, 5270, Slovenia*

[e]*School of Natural Sciences, Ryan Institute's Centre for Climate and Air Pollution Studies, University of Galway, H91 CF50 Galway, Ireland*

[f]*GEMMA and POLARIS Research Centres, Department of Earth and Environmental Sciences, University of Milano-Bicocca, Milano, 20126, Italy*

© 2026 The Author(s). Published by the Royal Society of Chemistry

BBOA, highlighting the potential for nocturnal multiphase chemistry to generate absorbing secondary BrC.[8] Global modelling and observations suggest that a distinct class of 'dark BrC' with stronger visible-near-infrared (IR) absorption can contribute substantiallt toa positive radiative effect, implying that OA absorption may be underestimated when models omit these more strongly absorbing BrC components.[9]

To study the nocturnal formation of BrC and provide real-world observations for integration into models, we conducted a measurement campaign in the Po Valley, one of Europe's air pollution hotspots. Especially during autumn and winter, when stable atmospheric conditions and low wind speed lead to aerosol accumulation within the planetary boundary layer,[10,11] pollution events are even visible from satellite observations (Fig. S1).[12–15] In order to improve air quality, open field burning of agricultural and forest residues was banned in the Lombardy region in compliance with European regulations to improve air quality.[16,17] Despite these measures, BB is still a substantial source of OAs in the region, with the sources, effects and temporal dynamics of BrC remaining insufficiently understood and under active investigation.

To gain a better understanding of OA composition and BrC formation in the rural agricultural Po Valley, we conducted high-resolution chemical profiling of OA in Schivenoglia (SKI; Lombardy region; 45°01′0.8″ N 11°04′33.7″ E) during autumn 2023. For chemical characterization we used online atmospheric pressure chemical ionization coupled with Orbitrap mass spectrometry (APCI-Orbitrap-MS) and an aerosol chemical speciation monitor (ACSM).[18] This setup provides detailed molecular-level insights into OA composition,[18] helping to understand and deconvolute the complex temporal dynamics of short-lived BB events. Simultaneously, continuous measurements of the optical properties of LAA (BC and BrC) were conducted using an Aethalometer (AE36s) across an extended short wavelength spectrum (400, 370, and 340 nm). By integrating these complementary approaches, we were able to resolve temporal trends in OA composition and identify molecular markers of BrC, thereby establishing a direct connection between chemical composition and observed variations in BrC light-absorbing behaviour.

Methods

Field site description and instrumentation Schivenoglia (Po Valley, Italy)

From 28 September to 12 October 2023, the measurement campaign was carried out in Schivenoglia (SKI, 45°01′00.8″ N 11°04′33.7″ E), an agricultural site in the Po Valley, Italy. A laboratory container was located on the side of agricultural fields next to the measurement site of ARPA (Agenzia Regionale per la Protezione dell' Ambiente) Lombardia.[19] The measurement site is about 200 m from the Canale della Bonificia Reggiana Montovana and ∼2.7 km from the Po river. The closest village to the measurement container is Schivenoglia within ∼2 km distance. A few individual farms were located closer to the field site. During the campaign, most of the surrounding fields had already been harvested, with only a few crops still standing in the fields. In some cases, fields were being ploughed, or manure was spread. The measurement container was equipped with a $PM_{2.5}$ particle inlet (Digitel AG), which was installed 2 m above the container roof and was made of stainless steel. All particle measurement devices, including the APCI-Orbitrap-MS, ACSM, scanning mobility particle sizer (SMPS) and AE36s were connected to a stainless-steel laminar flow splitter with stainless steel tubing (Fig. S2).

Online aerosol mass spectrometry

For the online chemical analysis of non-refractory submicron particles, two instruments were placed in the mobile laboratory container. The time of flight aerosol chemical speciation monitor (ToF-ACSM, Aerodyne Research Inc.), provided quantitative data for ambient aerosol[20] whereas an Atmospheric Pressure Chemical Ionization Orbitrap Mass Spectrometer (APCI-Orbitrap-MS, Exploris 120 by Thermo Fisher Scientific Inc.), provided molecular level information.[18] Briefly, as described by David *et al.* (2025), the APCI-Orbitrap-MS recorded one complete spectrum per second and was operated at 1.6 L min^{-1} from which the gas phase was removed with a multichannel charcoal denuder. The particle phase is vaporized at 350 °C in a heated ceramic tube and subsequently the molecules are ionized *via* a corona discharge.[18] The main ionization pathways are protonation and deprotonation in positive ($APCI_{pos}$) and negative ($APCI_{neg}$) ionization mode, respectively. Protonation is especially favourable for organic compounds with functional groups having a lone electron pair. Deprotonation is especially favourable for multifunctional organic molecules with acidic protons.[18,21–23] The ToF-ACSM is a widely used instrument for the continuous monitoring and quantification of organic aerosol. The ACSM can determine the mass concentration of the main non-refractory species in submicrometre particles fraction (near-PM_1), namely organics, nitrate, sulphates, ammonium, and chloride. This is obtained by thermal particle vaporization at 600 °C in a standard vaporizer chamber, followed by electron ionization (EI) at 70 eV and detection by a compact ToF-MS.[20]

Online APCI-Orbitrap-MS data processing

We used Orbitool 2.5.2 beta[24] for processing online APCI-Orbitrap-MS data, applying a mass tolerance of ±1.5 ppm and averaged over 10 min for comparability with other instruments. The molecular formulae were calculated using the following criteria: number of carbon atoms (#C = 0−30), hydrogen atoms (#H = 0−60), oxygen atoms (#O = 0−15), nitrogen atoms (#N = 0−10), sulphur atoms (#S = 0−10), and phosphorus atoms (#P = 0−10). For the molecular formulae generated by Orbitool, we additionally applied plausibility filters to eliminate implausible molecular formulae. The filters included the following criteria: the DBE cannot be negative or a non-integer value, an O/C and H/C ≤ 3, and O/P ≥ 3. The dataset was background-corrected by conducting regular zero measurements by redirecting the sample flow through an HEPA filter for a minimum of 30 minutes (Table S1). Each compound was subsequently background corrected by recording its average signal background

© 2026 The Author(s). Published by the Royal Society of Chemistry

and then subtracting it from the measured signal intensity. For further analysis compounds with 99% or more missing values were excluded.

The volatility of compounds was calculated according to eqn (1) and Table S2.

$$\log_{10} C_0 = \left(n_C^0 - n_C\right)b_c - n_O b_O - 2\frac{n_C n_O}{n_C + n_O}b_{CO} - n_N b_N - n_S b_S \quad (1)$$

with n_C^0 as the reference carbon number, $n_{C,O,N,S}$ as the number of carbon, oxygen, nitrogen and sulfur atoms. $b_{C,O,N,S}$ denote the contribution of each atom to $\log_{10}C_0$ and b_{CO} being the carbon-oxygen nonideality.[25–27]

Hierarchical cluster analysis

We conducted a hierarchical cluster analysis (HCA), using the background-corrected time series, to reduce the dimensionality of the complex mass spectrometric dataset. The HCA groups individual compounds into clusters that exhibit similar temporal behaviour. For this, the intensity time series of each extracted ion chromatogram (EIC) was individually normalized using *z*-transformation, which standardizes each series based on its mean intensity and variance over the entire period. The resulting normalized dataset is visualized as a heatmap. Following normalization, pairwise distances between compounds were calculated using Euclidean distance and Ward linkage, providing a measure of similarity or dissimilarity between time series. Larger distances correspond to greater differences in compound temporal patterns. The input matrix consisted of EICs for compounds with unambiguous molecular formula assignments from both $APCI_{neg}$ and $APCI_{pos}$ measurements.[28] The HCA were performed in MATLAB R2024b (The MathWorks).

ACSM data processing

To analyse the ToF-ACSM data, we used Tofware (version 4.0.0) within the Wavemetrics Igor Pro (version 7) environment. Default ionization efficiency (IE) values were applied for nitrate (1.05), organics (1.4), and chlorine (1.3). Based on field calibrations, collection efficiency of the standard vaporizer was estimated using the composition-dependent collection efficiency (CDCE) approach.[29] The ammonium detection limit was calculated as 0.5 μg m^{-3} based on three times the standard deviation over a 3 hour period with an HEPA filter installed before the ACSM inlet.

SMPS data processing

SMPS data quality was ensured by frequent leak-tightness checks. For this, the SMPS was placed behind the same HEPA filter used for background correction of the APCI-Orbitrap-MS signal. Frequent zero measurements confirmed that only ambient particles were sampled.

Particle density in general is highly variable but has been reported to average around 1.4 ± 0.5 and 1.5 ± 0.5 g cm^{-3} for $PM_{2.5}$.[3] For the particle mass calculations a for organic aerosol typical particle density of 1.5 g cm^{-3} was assumed.[30,31]

AE36s measurements and HR calculation

To determine the aerosol heating rate (HR), measurements of the aerosol absorption coefficient b_{abs} must be taken at multiple wavelengths within the UV-VIS-NIR range. The AE36s (M8060 filter tape) was used to assess $b_{abs}(\lambda)$ at 1 min time resolution at nine different wavelengths: 340, 370, 400, 470, 520, 590, 660, 880 and 950 nm.

The AE36s measures the attenuation (ATN) of light (at each wavelength transmitted) through a particle laden filter spot and through a sample free portion of the tape and has the same principle of operation as the previous model AE33.[32] ATN is calculated as:

$$\mathrm{ATN} = 100\ln(I_0/I) \quad (2)$$

where I_0 and I are the intensity of light transmitted through the reference and aerosol spot of the filter, respectively. The attenuation coefficient of the aerosol particles, $b_{ATN}(\lambda)$, is then determined:[33]

$$b_{ATN}(\lambda) = \frac{A}{Q}\frac{\Delta\mathrm{ATN}(\lambda)}{100\Delta t} \quad (3)$$

where A is the filter spot area, Q the volumetric flow[34] rate and $\Delta\mathrm{ATN}(\lambda)$ is the change in attenuation during the time interval Δt. In the Aethalometer AE33 and subsequent models (among which AE36s), a DualSpot technology has been integrated and an internal algorithm compensates for the loading effect,[32] by determining the loading parameter k in real-time. Subsequently, AE36s, estimates the absorption coefficient that, together with the inner nominal mass absorption cross-section of 7.77 m^2 g^{-1} at 880 nm provide the BC concentrations as eBC (nominal equivalent BC) in keeping with Petzold *et al.* (2013) and Savadkoohi *et al.* (2024).[3,34] However, a reliable determination of $b_{abs}(\lambda)$ compensation for the multiple scattering of the light induced by the filter fibres and by the particles embedded in it is required; its determination is referred to the parameter C which compensates for it. C can be determined using parallel reference absorption instruments.[33,35–38] Neither a common accepted unique reference instrument[3,39,40] nor reference material[41] exist for the measurement of $b_{abs}(\lambda)$, and commonly used standard online (CAPS, MAAP, PAX, PTAAM) and offline (MWAA)[42,43] reference devices are not available at each measuring site around the world. Therefore, the ACTRIS community[44] suggested to use a C value of 2.45 for the AE33 and other Aethalometers equipped with M8060 filter tape. The advantage is the comparability of results obtained in different sites. However, the real C values can vary greatly as they depend on chemical composition and therefore can vary between different environments, *e.g.* in the 2.23–4.24 range.[45–47] Therefore, the use of a constant harmonizing C value in different seasons and locations will influence the determination of the absorption coefficient, reflecting on the single scattering albedo and therefore on the resulting climatic forcing and heating rate.[46,48] Thus, the C parameter was determined through a novel methodology that provides a MAAP-like C from the Aethalometer loading parameters k as follows:[49]

© 2026 The Author(s). Published by the Royal Society of Chemistry

$$C_{AE} = C_{ref} + \alpha_{AE}\frac{m \times (1 - 50 \times k) - 50 \times k}{50 \times k} \quad (4)$$

where C_{AE} refers to the C obtained directly from the AE33 k data, C_{ref} and α_{AE} are the reference multiple-scattering filter parameter (that depends only on the filter properties) and the scattering fraction parameter which equals 2.306(±0.018) and 0.033(±0.003), respectively.

Thus, $b_{abs}(\lambda)$ values are retrieved as follows:

$$b_{abs(\lambda)} = \frac{b_{ATN_LC(\lambda)}}{C_{AE}} \quad (5)$$

where $b_{ATN_LC}(\lambda)$ is the attenuation coefficient already corrected for the loading effect,[32] and C_{AE} is obtained from eqn (4); to the campaign-average is 2.40 ± 0.01, similar to the ACTRIS aforementioned recommendation and within the reported C range. Moreover, it is reasonable for the present campaign due to high fraction of absorbing aerosol occurring during the BB emission discussed in the present work. Once $b_{abs}(\lambda)$ are determined, they can be: (1) apportioned for carbonaceous species (*i.e.* black and brown carbon, BC and BrC) and (2) used as a whole or in the apportioned form to determine the atmospheric HR due to the absorbing aerosol released in the atmosphere. Starting with the apportionment, from a general point of view, any traditional apportionment of the species and sources is based on three equations:

$$\frac{b_{abs}(\lambda_1)_A}{b_{abs}(\lambda_2)_A} = \left(\frac{\lambda_1}{\lambda_2}\right)^{-AAE_A} \quad (6)$$

$$\frac{b_{abs}(\lambda_1)_B}{b_{abs}(\lambda_2)_B} = \left(\frac{\lambda_1}{\lambda_2}\right)^{-AAE_B} \quad (7)$$

$$b_{abs}(\lambda_{1,2}) = b_{abs}(\lambda_{1,2})_A + b_{abs}(\lambda_{1,2})_B \quad (8)$$

where A and B represent two different LAA species (BC, BrC) or sources (FF, BB), λ_1 and λ_2 are two different wavelengths and AAE_A and AAE_B are the specific absorption Angstrom exponents. If AAE_A and AAE_B are chosen *a priori* as well as λ_1 and λ_2, we are in the case of the so-called Aethalometer model for FF and BB apportionment.[37] If AAE_A is chosen *a priori* and only λ_2 is used, as in Tian *et al.* (2019), the method allows a BC/BrC apportionment. In this approach, $b_{abs}(\lambda)_{BC}$ is calculated assuming, for example, that $b_{abs}(950)_{BrC} = 0$ and $AAE_{BC} = 1$. Therefore, $b_{abs(\lambda)_BrC}$ is obtained as difference between the total absorption and BC absorption and AAE_{BrC} is estimated accorningly.[50] It is worth noting that this apportionment remains a mathematical solution and can be affected by real-world mixing states; in biomass burning aerosol, internally mixed BrC–BC can induce BrC-driven suppression of BC lensing, leading to $AAE_{BC} < 1$ when coatings are thick,[47] which may influence the retrieval of $b_{abs}(\lambda)$ for individual species.

If finally, λ_1 and λ_2 are not chosen *a priori*, but all possible Aethalometer wavelengths are used, two methods can be applied by fitting $b_{abs}(\lambda)$ over the whole spectrum: the multi-λ fit approach reported in Bernardoni *et al.*, 2021 or the MWAA (Multi-Wavelength Absorption Analyzer) model described in previous works.[42,51,52] More recently, Ivančič *et al.* (2022) went deeper in the wavelength driven apportionment method for Aethalometers and used first eqn (8) for splitting $b_{abs}(\lambda)$ between BC and BrC contribution on the base of Tian *et al.*, (2019) approach ($b_{abs}(880)_{_BrC} = 0$ in keeping with the discoveries of Ferrero *et al.* (2021a) related to uncertainties in 950 nm) and then $b_{abs}(\lambda)$ of both primary and secondary BrC (BrCp and BrCs, and the related $b_{abs}(\lambda)_{_BrCp}$ and $b_{abs}(\lambda)_{_BrCs}$, respectively) is obtained again on the basis of eqn (8) after the computation of $b_{abs}(\lambda)_{_BrCs}$ with time as follows:[5,50,53]

$$b_{abs}^{BrCs}(,t) = b_{abs}(,t) - \left(\frac{b_{abs}(\lambda)}{b_{abs}(\lambda_0)}\right)_{prim} \times b_{abs}(\lambda_0, t) \quad (9)$$

where l_0 = 880 nm (as aforementioned) and the ratio $\left(\frac{b_{abs}(\lambda)}{b_{abs}(\lambda_0)}\right)_{prim}$ represents the ratio of absorption at all wavelength (compared to 880 nm) only due to the presence of primary absorbing BrCp material; the ratio $\left(\frac{b_{abs}(\lambda)}{b_{abs}(\lambda_0)}\right)_{prim}$ is obtained *via* a statistical approach by varying its hypothetical value from zero and above with step of 0.1 and determining it by minimizing the correlation between $b_{abs}(\lambda,t)_{_BrCs}$ and $b_{abs}(\lambda_0,t)_{_BrCs}$. Further details are reported in Ivančič *et al.* (2022).

Once the total $b_{abs}(\lambda,t)$ and its apportioned values ($b_{abs}(\lambda,t)_{_BC}$, $b_{abs}(\lambda,t)_{_BrCp}$ and $b_{abs}(\lambda,t)_{_BrCs}$) are known, it is possible to compute the $HR(t)_x$ as:

$$HR_x(t) = \frac{1}{\rho C_p} \times \sum_{n=1}^{3} \int_\theta \int_\lambda \frac{F_n(\lambda, t, \theta)}{\cos\theta} b_{abs}(\lambda, t) d\lambda d\theta \quad (10)$$

where x represents the total HR as a whole ($HR_{tot}(t)$) or the one obtained by $b_{abs}(\lambda,t)$ apportionment: $HR_{BC}(t)$, $HR_{BrC}(t)$, $HR_{BrCp}(t)$ and $HR_{BrCs}(t)$; then r represents the air density (kg m^{-3}), C_p (1005 J kg^{-1} K^{-1}) is the isobaric specific heat of dry air, n is the index indicating the nth type of radiation (n stands for direct, diffuse or reflected) impinging the absorbing aerosol, λ and θ represent the wavelength and zenith angle of the radiation and t is the time.

The instantaneous aerosol HR was then determined by combining the LAA multi-wavelength absorption coefficient ($b_{abs}(\lambda)$) and radiation data obtained from the ARPA local station, Copernicus service and Nasa albedo of the surface. Details of the methodology are reported in Ferrero *et al.* (2018, 2021a, b, 2024).

Finally, it is noteworthy that eqn (10) can be rewritten as follows:[46]

$$HR_x(t) = \frac{1}{C} \times \frac{1}{\rho C_p} \times \sum_{n=1}^{3} \int_\theta \int_\lambda \frac{F_n(\lambda, t, \theta)}{\cos} b_{ATN_LC(\lambda,t)} d\lambda d\theta \quad (11)$$

thus showing that, once the HR with a C value has been determined (*i.e.* $C_{AE} = 2.40 \pm 0.01$ in our case), it is possible to rescale the data using a different C in case of future more accurate determination and easily determine the new HR values for long-term data series harmonization of radiative forcing and HR in different world sites; this procedure, however, does not influence the temporal behaviour, the relative contribution of $HR_{BC}(t)$, $HR_{BrC}(t)$, $HR_{BrCp}(t)$ and $HR_{BrCs}(t)$.

© 2026 The Author(s). Published by the Royal Society of Chemistry

Results and discussion

Distinct chemical fingerprisnts of transient and sustained organic aerosol

During the campaign, we detected several transient BB plumes, with individual plumes lasting from only a few minutes up to several hours. In contrast to traditional approaches of OA characterisation with lower temporal resolution (*e.g.* filter sampler with 12 or 24 h resolution), our measurements enabled the detection of short and small-scale burning events. This high time resolution allowed us to capture the influence of transient BB events on local air quality and aerosol properties.

BB events are characterized by the emission of thousands of distinct compounds to which we applied HCA. As basis we use molecular-resolved OA composition measurements, which represents the intensity of individual species over time. In short, the HCA is used for reducing the dimensionality of complex mass spectral datasets by grouping individual compounds together according to the similarity of their temporal behaviour (Fig. 1). In the HCA, compounds are grouped based on similarity in their temporal covariance patterns, yielding mutually exclusive clusters for the purpose of classification, although individual species can originate from multiple sources and/or atmospheric processes.[28] Unlike positive matrix factorization (PMF), the HCA does not require a calibrated dataset with an error matrix.

During the first measurement period (28 September–05 October 2023), we operated the system in $APCI_{neg}$ mode, identifying and simultaneously monitoring approximately 1200 compounds. To obtain more comprehensive measurements, the system was operated in $APCI_{pos}$ during the second period (05–12 October 2023), where approximately 1780 compounds were detected (Fig. 1a and b). The HCA shows that both periods were strongly influenced by BB events, with up to 80% of the detected organic molecules being related to BB. During the two-week continuous measurement, ten BB events were observed across all instruments (Fig. S3). Although these BB events occurred frequently during the campaign, it cannot be directly deduced that this pattern will continue throughout the year. BB events in the HCA are marked by high-intensity periods (dark red), during which the ACSM organics and the SMPS show peak mass concentrations of up to 137 μg m^{-3} and 80 μg m^{-3} on a ten-minute average. On a two-minute average, peak concentration up to 183 and 236 μg m^{-3} were detected, highlighting the transient character of the BB events (Fig. S4), being associated with a large measurement uncertainty. Particle sizes

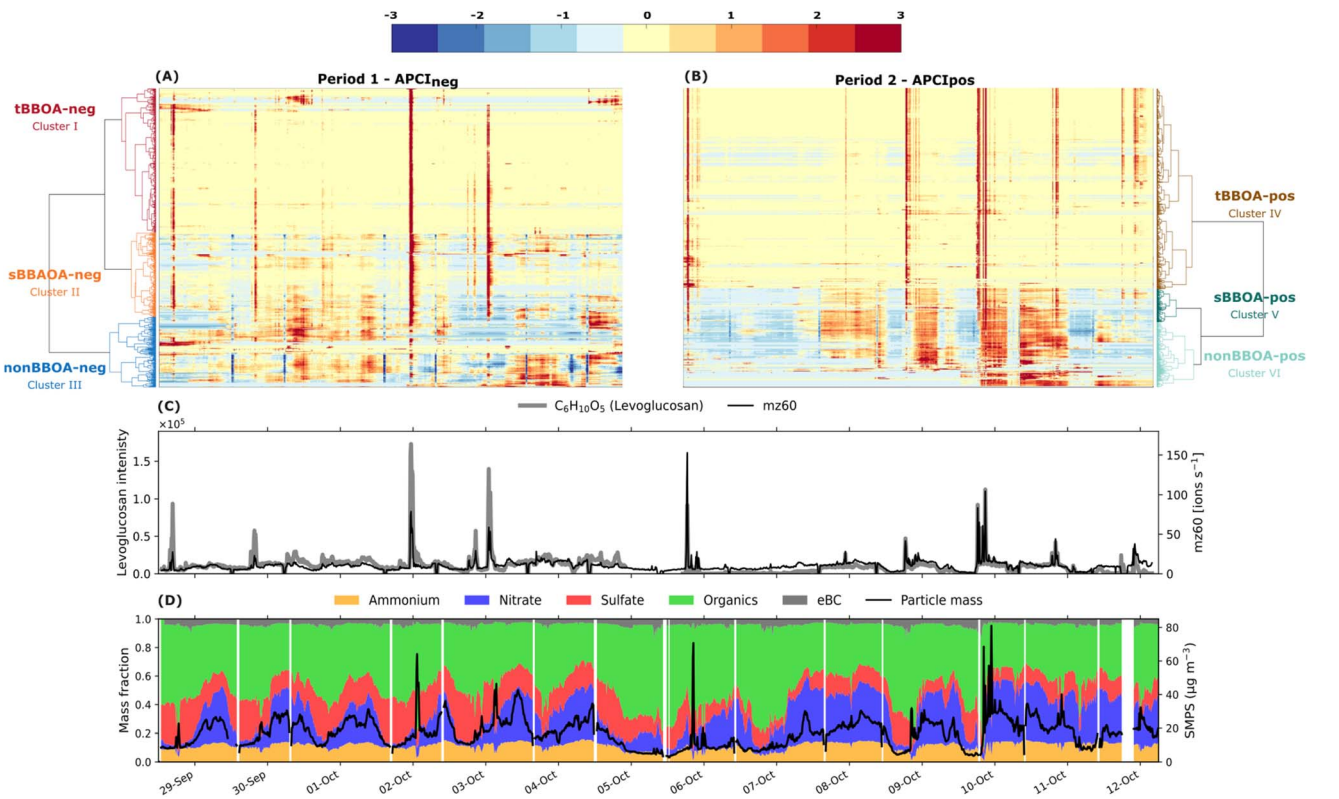

Fig. 1 Time Series of organic aerosol composition for (A) Period 1 ($APCI_{neg}$) and (B) Period 2 ($APCI_{pos}$) measured by APCI-Orbitrap-MS visualized as a hierarchical cluster analysis (HCA). Heatmap colours represent z-score standardized, background-corrected intensities of detected compounds, with clustering performed along the *y*-axis. Note that clustering across polarities was not performed due to differences in sensitivity between the APCI-Orbitrap-MS acquisition modes. (C) Timeseries of $C_6H_{10}O_5$ (Levoglucosan and isomers; grey) measured by the APCI-Orbitrap-MS on the left *y*-axis. Additionally, *m*/*z* 60 a characteristic fragment for levoglucosan (and isomers; black) measured by the ACMS in ions s^{-1} on the right *y*-axis. (D) Mass fraction plot for ammonium (orange), nitrate (blue), sulphate (red), organics (green) and equivalent black carbon (eBC; grey), as well as the particle mass concentration measured by the SMPS in μg m^{-3} (black). All data is averaged over 10 minutes.

© 2026 The Author(s). Published by the Royal Society of Chemistry

Table 1 Characteristics of cluster identified with the HCA showing their respective measured polarity ($APCI_{neg}$ & $APCI_{pos}$), cluster number and attributed cluster names along with the average oxygen to carbon (O/C), hydrogen to carbon (H/C) and oxidation state of carbon $\overline{OS}_C$. Number and percentage of attributed formulae per cluster for CHO, CHON, CHOS, CHN and Others, respectively and total number of compounds (# Comp.) per cluster

Polarity	Cluster nr.	Cluster name	O/C	H/C	$\overline{OS}_C$	CHO	CHON	CHOS	CHN	Others	# Comp.
$APCI_{neg}$	Cluster I	tBBOA-neg	0.24	1.37	−0.89	n = 208; 35.5%	n = 344; 58.7%	n = 2; 0.3%	n = 0; 0%	n = 11; 1.9%	586
	Cluster II	sBBOA-neg	0.63	1.04	0.23	n = 114; 40.7%	n = 159; 56.8%	n = 2; 0.7%	n = 0; 0%	n = 3; 1.1%	280
	Cluster III	nonBBOA-neg	0.7	1.43	−0.03	n = 238; 66.3%	n = 79; 22%	n = 22; 6.1%	n = 0; 0%	n = 3; 0.8%	359
$APCI_{pos}$	Cluster IV	tBBOA-pos	0.17	1.47	−1.14	n = 412; 36.1%	n = 544; 47.7%	n = 4; 0.4%	n = 112; 9.8%	n = 58; 5.1%	1141
	Cluster V	sBBOA-pos	0.56	1.21	−0.09	n = 74; 39.4%	n = 110; 58.5%	n = 0; 0%	n = 0; 0%	n = 1; 0.5%	188
	Cluster VI	nonBBOA-pos	0.65	1.56	−0.26	n = 137; 37.1%	n = 215; 58.3%	n = 3; 0.8%	n = 5; 1.3%	n = 5; 1.4%	369

during the events show an increase of the mode diameter larger than 100 nm (Fig. S5). Fig. 1c shows the timeseries of levoglucosan (and isomers), a well-known and characterised BB tracers, as well as the m/z 60, a commonly used fragment detected by the ACSM as a proxy of levoglucosan.[54,55] Both measurements for levoglucosan, with the APCI-Orbitrap-MS and the ACSM correlate significantly with an $r = 0.9$ and $r = 0.87$ in $APCI_{neg}$ and $APCI_{pos}$, respectively (Fig. S6). Additional correlations between BB events, represented by detected levoglucosan, are shown for the cluster analysis and absorption measurements in Fig. S6. Fig. 1d shows the mass fraction of the ACSM non-refractory chemical species and the equivalent black carbon concentration (eBC). During period 1, a clear diurnal pattern is evident in both the APCI-Orbitrap and ACSM measurements (Fig. S7), with the ACSM organic mass fraction peaking during the day (Fig. 1d). However, looking at the diurnal cycle of particle mass in Fig. S7 reveals that both the ACSM organics and the nitrate have the highest concentration during the night until noon, after which they drop considerably likely due to planetary boundary layer dynamics.

In period 2, this diurnal behaviour breaks down and is no longer apparent, with more stable atmospheric conditions over longer periods. eBC shows an average level of 1.68 ± 0.01 μg m^{-3} (Fig. S8) and overall follows closely the time series of aerosol mass.

The molecular fingerprints (Fig. S9) of each cluster identified in the HCA (Fig. S10) illustrate the chemical composition of the compounds with similar temporal behaviour. The van Krevelen diagram shows the atomic oxygen to carbon (O/C) against the hydrogen to carbon (H/C) ratios while the Kroll plot shows average oxidation state of carbon [$\overline{OS}_C$ =2 O/C − H/C] as a function of carbon-atom count.[56] The 20 compounds with the highest intensity are shown and characterised in Table S3 for each cluster.

The HCA identified three main clusters in $APCI_{neg}$ mode, of which two were associated with BB influences, while the third is attributed to SOA formation.

Compounds within cluster I are biomass burning organic aerosol (BBOA) compounds, which show a transient behaviour with peak intensities during BB events, and low intensities, in some cases below the instrumental noise level, between BB events. This cluster will therefore further refer to as transient BBOA compounds detected in negative ionisation mode (tBBOA-neg).The tBBOA-neg cluster comprises 586 compounds as shown in Table 1 and Fig. S11 with predominantly nitrogen-containing organic compounds (CHON; n = 344) and organic compounds (CHO; n = 208). The compounds within this cluster have an average O/C ratio of 0.24, an average H/C of 1.37, and average $\overline{OS}_C$ of −0.89. These values agree with typical values for primary emitted BBOA described by Aiken *et al.* (2008).[57] Some notable BB markers here are $C_8H_8O_3$ (vanillin, confirmed by MS^2), which is emitted during the pyrolysis of lignin,[58] $C_9H_{10}O_5$ (possibly syringic acid) and $C_{18}H_{36}O_2$ (possibly stearic acid). Noticeable for this cluster are several high-molecular weight CHO compounds (>C_{15}), typically linked to flaming conditions during burning,[59] often resulting from the pyrolysis of cell walls and membranes.[60–62]

© 2026 The Author(s). Published by the Royal Society of Chemistry

Cluster II is, similar to tBBOA-neg, strongly influenced by BB, but shows a significantly different temporal behaviour. Compounds in cluster II exhibit the highest intensities during BB events and maintain elevated levels afterwards and will therefore be referred to as sustained BBOA compounds detected in negative ionisation mode (sBBOA-neg). The sBBOA-neg cluster contains 280 compounds, primarily CHON ($n = 159$) and CHO ($n = 114$). The average O/C ratio of compounds in cluster sBBOA-neg is 0.63, which exceeds the typical range of 0.3–0.4 for primary BBOA. Similarly with the average $\overline{OS}_C$ of 0.23, is substantially above the common range of −1 to −0.7 typically considered for BBOA,[56] and a rather typical range for secondary oxidation products.[57,63] Interestingly, levoglucosan ($C_6H_{10}O_5$, confirmed by MS^2), a widely known primary emitted BB marker,[58] is the highest intensity compound within this cluster, classifying it as a mixed cluster containing higher oxidized primary emitted compounds (*e.g.* anhydrosugars) as well as secondary oxidation products.

Cluster III is, in contrast to tBBOA-neg and sBBOA-neg, not influenced by BB events but is characterized by compounds associated with SOA formation from day- and nighttime chemistry. This cluster will be further referred to as non BBOA influenced compounds detected in negative ionisation mode (nonBBOA-neg). The nonBBOA-neg cluster contains 359 compounds and is the most diverse in molecular composition in terms of compound classes with CHO ($n = 238$), CHON ($n = 79$) and CHOS ($n = 22$). Its chemical composition falls within the typical range described for biogenic SOA with an average O/C of 0.7 and H/C of 1.43. It contains typical marker of daytime SOA formation and aerosol aging such as $C_8H_{12}O_6$ (3-methyl-1,2,3-butanetricarboxylic acid; MBTCA; confirmed by MS^2),[64,65] while $C_8H_{13}O_8N$ is a marker for nighttime chemistry with high peak intensities during the night and low intensities during the day (Fig. S7).[18,66] Additionally, based on assigned molecular formulae several potential light absorbing secondary monoterpene oxidation products possibly from NO_3 oxidation occur within this cluster including $C_9H_{13,15}O_8N$, $C_{10}H_{13}O_{6,8}N$, $C_{10}H_{15}O_{5,6,8}N$ and $C_{10}H_{17}O_8N$.[67]

Similar to the first measurement period, the HCA for $APCI_{pos}$ mode separates three main clusters from which the majority is linked to BB (cluster IV and V) whereas cluster VI can be characterized by compounds related to SOA formation.

Most compounds in cluster IV, further referred to as transient BBOA compounds detected in positive ionisation mode (tBBOA-pos), are directly linked to BB containing the highest number of compounds ($n = 1141$). It is composed mainly of CHNO ($n = 544$), CHO ($n = 412$), CHN ($n = 112$) and others ($n = 58$). It is noteworthy that $APCI_{pos}$ mode has an enhanced sensitivity to CHON and reduced sensitivity to CHOS compounds, additionally ionizes CHN compounds, which cannot be ionized in $APCI_{neg}$ mode due to the absence of acidic protons. High-intensity compounds in this cluster include $C_5H_8N_2$ (possibly dimethylimidazole), $C_9H_{16}N_2$ which was reported from the burning of dung and brushwood,[68] $C_6H_{10}N_2$ and $C_7H_{12}N_2$ reported from the pyrolysis of pine needles and sticks and southern California ceanothus.[69] Among CHO compounds is $C_{10}H_{10}O_3$ (possibly coniferylaldehyde), a compound reported for smouldering emissions.[59,68,69] Cluster V, similarly to sBBOA-neg, shows a sustained behaviour and will be referred to as sustained BBOA detected in positive ionisation mode (sBBOA-pos). sBBOA-pos has the least attributed compounds ($n = 188$), consisting mainly of CHNO ($n = 110$) and CHO ($n = 74$) compounds. Despite the higher number of CHON compounds, CHO compounds show higher intensities (Fig. S11). Cluster VI, further referred to as non BBOA compounds detected in positive ionisation mode (nonBBOA-pos), does in its evolution over time, very closely follow the overall OA mass. Compared to period 1, changes in meteorological conditions, in particular increasing wind speed, disrupted the regular diurnal cycles of PM, reducing $PM_{2.5}$ concentrations from on average ∼20 μg m^{-3} to approximately 5.3 μg m^{-3} on 8 October 2023 and 3.3 μg m^{-3} on 9 October 2023. Cluster VI mainly consist of CHNO ($n = 215$) and CHO ($n = 137$) and has very similarly to cluster nonBBOA-neg an average O/C of 0.65, average $\overline{OS}_C$ of −0.26 and an H/C of 1.56, alongside secondary BOA compounds from processes such as monoterpene oxidation (*e.g.*, $C_9H_{12}O_6$ likely from monoterpene oxidation).

Linking chemical composition to temporal dynamics and absorptive properties

A key characteristic visible in both ionization modes related to BB is the distinction in the temporal behaviour of BB signals. Transient signals, hereafter referred to as $BBOA_{trans}$, observed in clusters tBBOA-neg and tBBOA-pos, comprise compounds directly emitted during BB events, with negligible concentrations outside these periods. Concentrations of $BBOA_{trans}$ compounds rapidly decreases after the fires, possibly due to atmospheric processing such as aging and/or dilution. In contrast, sustained signals, hereafter referred to as $BBOA_{sus}$, represented by clusters sBBOA-neg and sBBOA-pos, exhibit the highest compound intensities during BB events and maintain at elevated concentrations even during non-BB periods. This behavioural difference is also evident in pollution plots, where $BBOA_{trans}$ (Fig. S12a and b) shows clear BB sources to the east of the measurement site, while $BBOA_{sus}$ (Fig. S12c and d) additionally reveals a regional background.[70,71] Notably, $BBOA_{sus}$ can be classified as a mixed sources cluster which includes compounds commonly classified in the literature as primary BB emissions, such as levoglucosan, alongside compounds associated with secondary BB formation. The presence of levoglucosan in $BBOA_{sus}$ does not imply secondary formation. Rather, it is consistent with aged BB influence, where primary emitted levoglucosan persists but at reduced concentrations, mixing with regional background concentrations. To explore the reasons behind these differences in the temporal evolution of the biomass burning plume, Fig. 2 displays all compounds combined for $BBOA_{trans}$ and $BBOA_{sus}$ across both polarities, with intensities normalized to the maximum measured value within each dataset.

Across both polarities, 1324 compounds showed transient behaviour and are therefore classified as $BBOA_{trans}$ compounds, while 372 compounds showed sustained pattern and are

© 2026 The Author(s). Published by the Royal Society of Chemistry

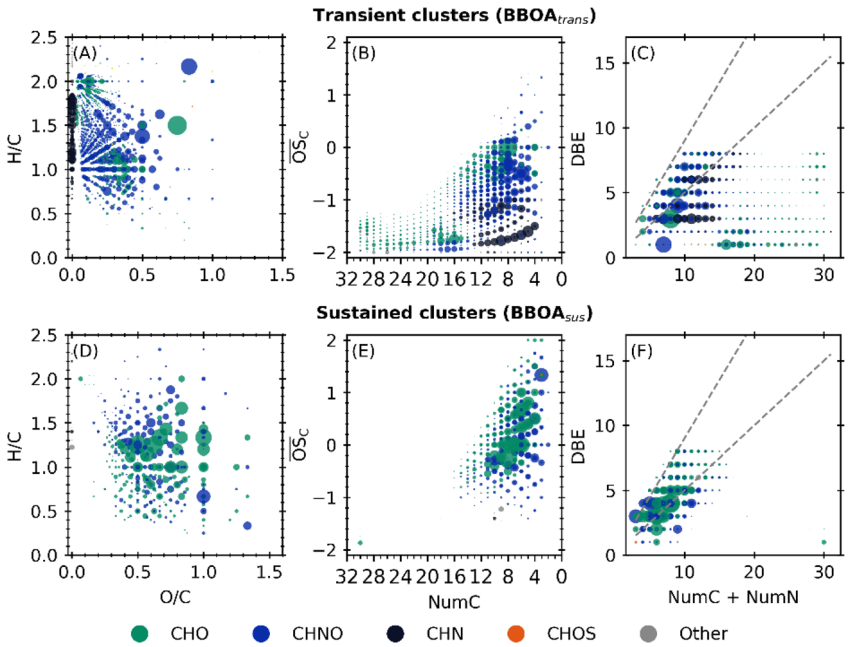

Fig. 2 A–C) BBOA$_{trans}$ compounds measured in the clusters I and IV and (D–F) BBOA$_{sus}$ compounds measured in the clusters II and V, with normalized signal intensity. (A + D) Van Krevelen plot with H/C against O/C; (B + E) Kroll plot with the average carbon oxidation state ($\overline{OS}_C$) against the number of carbon (NumC); (C + F) Double bond equivalent (DBE) plotted against the number of carbon and nitrogen atoms (NumC + NumN). Dashed lines as BrC-relevant space with DBE/(NumC + NumN) ratios ranging from 0.5 to 0.9. Upper boundary corresponds to fullerene-like hydrocarbons, lower boundary represents linear polyenes (C_XH_{X+2}).

classified as BBOA$_{sus}$. A clear difference between both clusters can be observed in terms of oxidative states. While lower oxidized compounds are commonly attributed to primary BBOA emissions, the higher oxidation levels are often associated with secondarily formed BBOA, due to oxidation processes. BBOA$_{trans}$ compounds have an average O/C ratio of 0.18 and $\overline{OS}_C$ of −1.10, whilst BBOA$_{sus}$ exhibits a higher oxidative state, with an average O/C ratio of 0.59 and an $\overline{OS}_C$ of 0.07. The average H/C ratio of BBOA$_{sus}$ is with 1.11 lower than BBOA$_{trans}$ with an H/C of 1.47 indicating a higher aromatic content. The main difference here is that BBOA$_{sus}$ especially has H/C values < 1 over a wider O/C range, also containing many CHO compounds, wheeas for BBOA$_{trans}$ most compounds are within a smaller O/C range.

While the measured compound intensity of BBOA$_{trans}$ is dominated by CHON compounds, contributing 57% to the overall cluster intensity, BBOA$_{sus}$ is dominated by CHO compounds with 61.4% followed by CHON with 38%, even though more distinct CHON species were detected in comparison to CHO. The high abundance of CHON compounds in both clusters indicate the burning of the poaceae family, such as corn and wheat plants rather than hardwood, as they mainly emit CHON[72] whereas the wood burning emits up to 90% CHO compounds.[59] The BBOA$_{trans}$ cluster additionally contains high amounts of CHN compounds (n = 112) which contribute to ~16% of the cluster intensity and are mostly $C_xH_yN_{\geq 2}$ and imidazole compounds, associated with fresh BB emissions.[73,74] Distinctive between the two behavioural patterns is additionally the number of carbon range. BBOA$_{sus}$ predominantly comprises smaller organic molecules, with carbon chain lengths ranging from C_3 to C_{15}, whereas the BBOA$_{trans}$ contains compounds up to C_{30}. These long chain compounds are often fatty acids, which can be emitted during active fires and originate from the pyrolysis of plant tissue.[60–62] These compounds are lost through fragmentation in the aging process.[59] Overall, BBOA$_{trans}$ is primary-like, enriched in primary BB tracers characterized by short peaks. In contrast, BBOA$_{sus}$ is more processed and/or secondary influenced, showing a more persistent behaviour, consistent with aging and/or mixed regional contributions. Estimating atmospheric lifetimes for the full clusters is not feasible due to their chemical diversity. Instead, vanillin and levoglucosan are used as representative compounds for the BBOA$_{trans}$ and BBOA$_{sus}$ clusters, respectively. Levoglucosan typically has a lifetime ranging from 1 to 4 days[75–77] with some studies suggesting lifetimes of up to 26 days under certain conditions.[78,79] This longer lifetime allows it to accumulate in the atmosphere. On the other hand, vanillin has a significantly shorter atmospheric lifetime of approximately 48.6 h in the presence of OH radicals and only 0.08 h when reacting with NO_3.[80] The fact that BB events occur during nighttime suggests that reactions with NO_3 radicals may contribute to the rapid decay of vanillin.[80,81] Note that based on these examples, it is not possible to assume the same behavior for the entire dataset, as the reactivity is not possible to be determined for all compounds.

Based on the parameterization by Donahue *et al.* (2011) and the extension by Li *et al.* (2016), we estimate the volatility distribution of all attributed molecular formula.[25–27] The majority of compounds can be classified as semi-volatile

© 2026 The Author(s). Published by the Royal Society of Chemistry

organic compounds (SVOC; 45% $BBOA_{trans}$ and 49% $BBOA_{sus}$), followed by intermediate volatility organic compounds (IVOC; 28% $BBOA_{trans}$ and 44% $BBOA_{sus}$) and as low volatility organic compounds (LVOC; 23% $BBOA_{trans}$ and 26% $BBOA_{sus}$). During BB events compounds across all volatility classes are emitted. The high organic mass loading during the BB events causes an increased partitioning of more volatile compounds, such as SVOC and IVOC, into the particle phase. After the passing of the BB plume, compounds can evaporate from particle phase, possibly explaining the transient observation of $BBOA_{trans}$ in the particle phase. The temporal behaviour of $BBOA_{sus}$, however, is influenced by additional factors such as temperature changes, dynamics of planetary boundary layer, relative humidity and atmospheric chemical reactions, affecting OA concentration and partitioning dynamics overnight.[25,26]

To link absorption measurements to molecular composition, organic molecules are typically considered absorptive when they contain delocalized π electrons.[6,82] As an approximation of absorptive behaviour, the double bond equivalent (DBE; $DBE = 1 + C - \frac{H}{2} + \frac{N}{2}$), provides the number of rings and double bonds within a molecule.[83] To evaluate the absorption properties of BBOA and determine whether they are absorptive, Fig. 2c and f show the DBE *versus* the total number of carbon and nitrogen atoms (NumC + NumN) for $BBOA_{trans}$ and $BBOA_{sus}$ compounds, respectively. Typical chromophores relevant for BrC absorption fall within a DBE to NumC + NumN ratio range of 0.5 to 0.9, known as the "BrC-relevant" absorption range.[43,84] For $BBOA_{trans}$ around 30.5% ($n = 404$) of compounds fall within the BrC-relevant range, compared to approximately 64.8% ($n = 241$) of $BBOA_{sus}$ compounds. For $BBOA_{trans}$ smaller and more oxidized compounds (up to C_{15}) predominantly lie within the absorption-relevant range, while larger, less oxidized aliphatic species ($>C_{15}$) generally fall outside. Chemical composition alone does not allow a direct quantification of a compound's light absorption. Instead, we can only infer its potential to absorb light. Accordingly, potential BrC-relevant compounds with the highest intensities in the $BBOA_{trans}$ cluster include $C_6H_{13}O_5N$, $C_8H_{11}O_4N$, and $C_5H_8N_2$, while in the $BBOA_{sus}$ cluster, the dominant compounds are CHO species such as $C_8H_{10}O_{4,5}$ and $C_6H_8O_4$. Additionally, several compounds previously reported in the literature as strong BrC absorbers were detected, including $C_9H_{10}O_3$ (acetovanillone isomer[43]), $C_8H_8O_3$ (vanillin isomer[43]), $C_8H_9O_4N$,[43,85] $C_7H_7O_4N$ (a methoxy-nitrophenol or methyl-nitrocatechol[43]) in the $BBOA_{trans}$ cluster. For the $BBOA_{sus}$ cluster we detected $C_9H_{10}O_4$ (isomer of syringaldehyde[43]), $C_8H_8O_4$ (vanillic acid isomer[43]), $C_8H_9O_5N$ (likely dimethoxy-nitrophenol[43]) and $C_6H_5O_4N$ (nitrocatechol[43,85]).

A common approach to quantify and characterize the absorption properties of BBOA is to describe the absorption spectra by analysing the BrC absorption wavelength dependence (from Aethalometer AE36s), which can be described by the absorption Ångström exponent (AAE_{BrC}). Absorption data were evaluated separately for BrCp and BrCs, which are distinguished by a conceptual optical split that may not fully align with the chemically defined clusters. Therefore, BrCs can comprise both secondary and aged BrC, consistent with the $BBOA_{sus}$ cluster, whereas BrCp closely corresponds to $BBOA_{trans}$. As a linkage between the two methods, the intensity of levoglucosan was used as a representative tracer for $BBOA_{sus}$, while vanillin is used for $BBOA_{trans}$. The AAE for BrC (AAE_{BrC}) was determined separately for BrCp and BrCs by fitting an exponential function to the absorption between 400 and 590 nm. Only periods where BrC absorption exceeded 15 Mm^{-1} and the exponential fit had $R^2 > 0.95$ were considered valid. In Fig. S13 AAE_{BrC} values were grouped by levoglucosan quartiles (Q1–Q4) and coloured by the normalized vanillin signal. In line with $BBOA_{trans}$ behaviour, BrCp is concentrated in the upper two levoglucosan quartiles (Q3–Q4) and occurs alongside elevated vanillin intensities, indicating fresh burning events. Consistent with $BBOA_{sus}$, BrCs is more frequent in the lower two levoglucosan quartiles (Q1–Q2) with low to no vanillin signal. Histograms of AAE_{BrC} show systematically higher AAE values for BrCp, peaking around 6–7, compared to BrCs, which peaks around 5–6. Saleh *et al.* (2020) classified AAE_{BrC} values in the range 5–8 as weakly absorptive brown carbon, typically associated with BrC produced under smouldering conditions.[86] This agrees with our APCI-Orbitrap-MS results, which detected compounds characteristic of smouldering fires. Cases with $AAE_{BrC} < 5$ occur predominantly in the Q1–Q2 levoglucosan quartiles and are linked to NO_3 driven oxidation processes, consistent with compounds detected in the $BBOA_{sus}$ cluster and previously reported for nighttime BBOA aging. Notably, both BrCp and BrCs exhibit higher absorption values during BB-events, consistent with the $BBOA_{sus}$ and $BBOA_{trans}$ clusters that also show their highest intensities under such conditions.

Linking chemical composition to local heating rates

The combination of molecular-level aerosol characterization by APCI-Orbitrap-MS and absorption measurements AE36s enables detailed investigation of the relationship between aerosol chemical composition and light absorption, providing high-resolution chemical and optical data critical for understanding the influence of BB on the air quality in the Po Valley.

To assess the radiative impact of these absorbing compounds, Fig. 3 links the temporal behaviour of compounds from $BBOA_{trans}$ (Fig. 3a) and $BBOA_{sus}$ (Fig. 3b) to the absorption across all wavelengths for primary (BrCp) and secondary BrC (BrCs), respectively. Both the absorption and intensity of $BBOA_{trans}$, as well as BrCp, show clear peaks during BB periods (indicated by the grey areas). Outside of BB periods, only minor contributions are observed, with a mean BrCp absorption of 4.8 Mm^{-1} ($\pm$10.8 Mm^{-1}, 1σ temporal variability). For $BBOA_{sus}$ and BrCs, similarly elevated absorption values are observed during BB periods. In contrast to $BBOA_{trans}$, a higher background level persists during non-BB periods, with a mean absorption of 9.9 Mm^{-1} ($\pm$11.3 Mm^{-1}, 1σ temporal variability). For light absorption by BrC compounds to occur, they must directly interact with solar radiation, leading to direct radiative effects (DRE in W m^{-2}) through the release of energy (heat) to the surrounding atmosphere, expressed as a heating rate (HR in K day^{-1}). Therefore, only compounds present during daytime,

© 2026 The Author(s). Published by the Royal Society of Chemistry

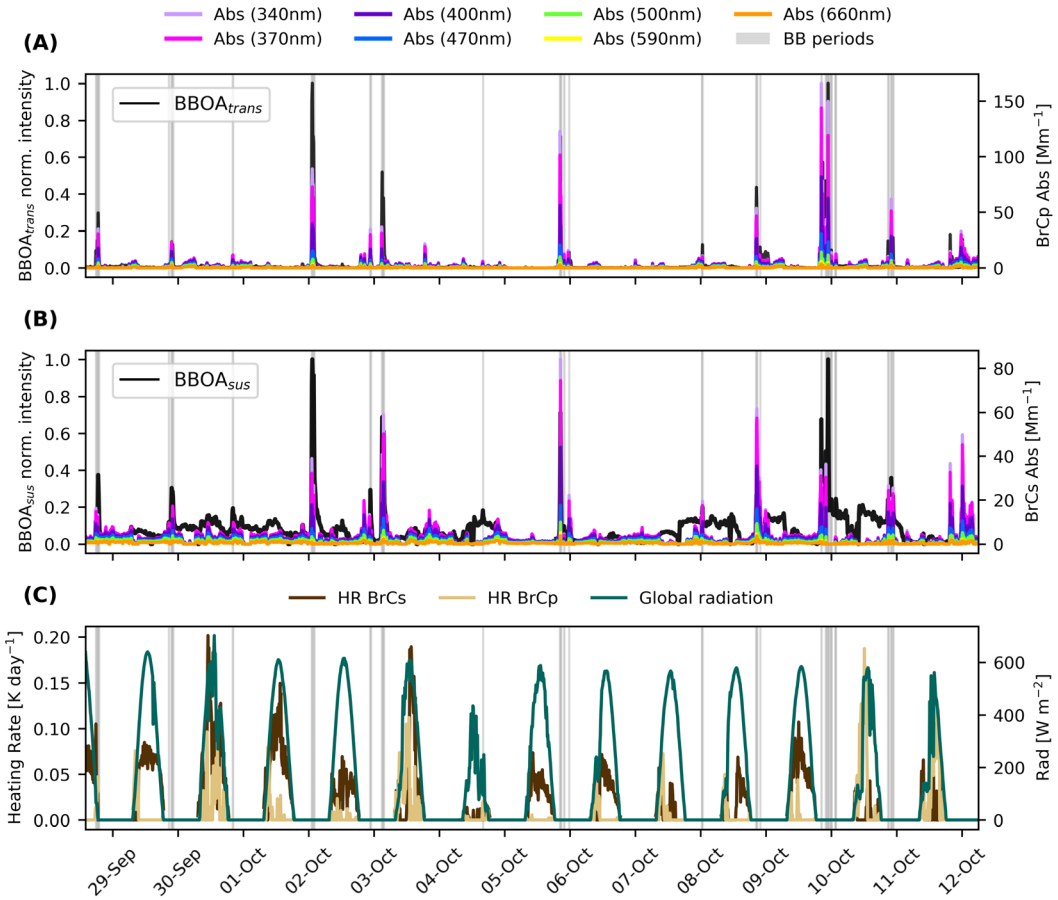

Fig. 3 (A) Normalized intensity of $BBOA_{trans}$ (black) as well as the absorption of BrCp across 340 to 660 nm in [Mm^{-1}]. (B) Normalized intensity of $BBOA_{sus}$ (black) as well as the absorption of BrCs across 340 to 590 nm in [Mm^{-1}]. (C) Heating rate (HR) in K day^{-1} for primary (HR_{BrCp}) and secondary (HR_{BrCs}) brown carbon calculated based on AE36s data, along with global radiation [W m^{-2}].

when solar radiation is available, can contribute to the HR. The total heating rate was calculated for BC ($HR_{BC}(t)$) and BrC ($HR_{BrC}(t)$), separated for primary brown carbon ($HR_{BrCp}(t)$) and secondary brown carbon ($HR_{BrCs}(t)$).[5,46] Fig. 3 c presents HR for primary ($HR_{BrCp}(t)$) and secondary BrC ($HR_{BrCs}(t)$), along with global radiation [W m^{-2}]. During nighttime, when global radiation (F_{glo}) is zero, no absorption-driven heating occurs. With sunrise and increasing F_{glo}, HR due to light absorbing aerosol rises. HR induced by LAA increases leading to a mean HR_{tot} of 0.609 ± 0.006 K day^{-1}, about half the autumn value previously observed by Ferrero *et al.* (2018) for Milan. In terms of species apportionment, HR_{BC} and HR_{BrC} contributed 0.565 ± 0.006 and 0.044 ± 0.001 K day^{-1}, respectively, accounting for $92.7 \pm 1.3\%$ and $7.3 \pm 0.1\%$ of total HR (Fig. S14).

As BB events occur predominantly at night, emitting BrCp and compounds in the $BBOA_{trans}$ clusters have only a minor influence on the HR. In contrast, BrCs which is mainly composed of compounds from the $BBOA_{sus}$ cluster drive most daytime heating, with the average ten minutes HR ranging from ~0.1 K day^{-1} under moderate radiation (~450 W m^{-2}) to ~0.2 K day^{-1} under stronger solar radiation (~600 W m^{-2}). These $BBOA_{sus}$ derived compounds are likely emitted at night and may undergo nocturnal oxidation with NO_3 radicals to form even more strongly absorbing species, which then efficiently absorb solar radiation during the day. Consequently, for the period investigated, HR was dominated by BrCs for $71.0 \pm 1.8\%$ (0.031 ± 0.001 K day^{-1}) with only $29.0 \pm 1.2\%$ attributed to BrCp (0.013 ± 0.001 K day^{-1}).

Conclusion

Our results revealed the strong influence of BB on the regional composition and $PM_{2.5}$ mass of OA in the Po Valley. Up to 80% of all identified organic compounds originated from nocturnal agricultural burning events, which occur despite existing bans on the burning of agricultural residue. Particularly noticeable is the difference in temporal evolution of BB compounds. We identified a subset of transient compounds ($BBOA_{trans}$) with lower oxidized compounds covering a wide size range of compounds, and a subset of higher oxidized compounds with sustained behaviour ($BBOA_{sus}$) that remains in the atmosphere. This dynamic and complex composition of compounds in ambient air highlights the need for measurements with high time and mass resolution.

Additionally, our results demonstrate that secondary BrC formed from nocturnal agricultural burning, rather than

© 2026 The Author(s). Published by the Royal Society of Chemistry

primary emissions, dominates the radiative heating impact of BrC in the rural Po Valley. Nocturnal BB emissions which are sustained in the residual layer, contribute more to daytime heating than the short peak in transient emissions themselves, challenging the common assumption that radiative impacts scale directly with total BB emissions, when secondary BrC from transient nighttime burning events accounts for 71.0 ± 1.8% of BrC-induced heating, driving a next-day heating rate of 0.031 ± 0.001 K day^{-1}. Therefore, parameterizations that tie BrC absorption solely to primary BB emissions are likely to underestimate heating rates in agricultural regions. Incorporating secondary BrC formation pathways and realistic diurnal emission timing will be essential to improve projections of regional climate and air quality. From a policy perspective, the results suggest that stricter enforcement of existing bans on open-field burning, together with the promotion of alternative residue management practices, would not only improve local air quality but also reduce BrC-induced heating in the valley. Because the strongest radiative impacts arise from emissions that occur under stable nocturnal conditions, targeted regulation of nighttime burns may offer a particularly effective lever to mitigate both health and climate impacts in agricultural regions.

Author contributions

JD wrote this paper, with ALV and LF advising on the writing process. JD, LD and ALV conceptualized the study. JD, LD, LF and ALV contributed to the laboratory and field measurements. Orbitrap data evaluation was performed by JD, AE36s data analysis and HR calculations were led by LF with the support of AG and MR, LD processed the ACSM data. ALV led the project administration. JD, ALV, LD, LF, VM, AG, MR provided feedback on the paper and contributed to the scientific discussions.

Conflicts of interest

Asta Gregorič and Martin Rigler are employees of Aerosol Magee Scientific selling the Aethalometer AE36s.

Data availability

The data analysed for this paper, as well as the supplementary information (SI), including the non-target analysis and the results of cluster analysis, are available on Zenodo at https://doi.org/10.5281/zenodo.21622888. Supplementary information: additional figures and a selection of the highest-intensity compounds per cluster. See DOI: https://doi.org/10.1039/d6ea00037a.

Acknowledgements

We acknowledge the GEMMA Center in the framework of project MUR TECLA “Dipartimenti di Eccellenza 2023–2027”. The authors thank ARPA Lombardia staff for the logistic support: in particular Giorgio Siliprandi, Lorenzo Mari, Enrico Bicelli and Rosario Cosenza. We want to thank Giorgio Siliprandi, Lorenzo Mari and Enrico Bicelli from ARPA Lombardia, as well as Mario Simon from the Goethe University, for their support during the SKI campaign. This research has been supported by the Deutsche Forschungsgemeinschaft (DFG; German Research Foundation) (grant no. 410009325). This project received funding by the European Regional Development Fund as part of the European Union's response to the COVID-19 pandemic (EFRE) 2014 to 2020 (IWB-EFRE Programme Hesse) – 20008794.

References

1 B. Domínguez, J. F. Nicolás, E. Mantilla, C. Gimeno, E. Borrás, M. Ródenas, T. Vera, R. Soler, M. Alfosea-Simón, E. Yubero, J. Crespo, N. Galindo, A. Clemente and A. Muñoz, Estimation of light absorption by secondary brown carbon during agricultural residues burning, *Atmos. Res.*, 2025, **325**, 108239.

2 T. S. Kapoor, G. Anurag, C. Navinya, S. Lonkar, K. Yadav, R. S. Raman, C. Venkataraman and H. C. Phuleria, Emissions from agricultural fires in India: field measurements of climate relevant aerosol chemical and optical properties, *Environ. Sci.: Atmos.*, 2025, **5**, 316–331.

3 A. Petzold, J. A. Ogren, M. Fiebig, P. Laj, S.-M. Li, U. Baltensperger, T. Holzer-Popp, S. Kinne, G. Pappalardo, N. Sugimoto, C. Wehrli, A. Wiedensohler and X.-Y. Zhang, Recommendations for reporting “black carbon” measurements, *Atmos. Chem. Phys.*, 2013, **13**, 8365–8379.

4 L. Ferrero, G. Močnik, S. Cogliati, A. Gregorič, R. Colombo and E. Bolzacchini, Heating Rate of Light Absorbing Aerosols: Time-Resolved Measurements, the Role of Clouds, and Source Identification, *Environ. Sci. Technol.*, 2018, **52**, 3546–3555.

5 L. Ferrero, A. Gregorič, G. Močnik, M. Rigler, S. Cogliati, F. Barnaba, L. Di Liberto, G. P. Gobbi, N. Losi and E. Bolzacchini, The impact of cloudiness and cloud type on the atmospheric heating rate of black and brown carbon in the Po Valley, *Atmos. Chem. Phys.*, 2021, **21**, 4869–4897.

6 A. Laskin, J. Laskin and S. A. Nizkorodov, Chemistry of atmospheric brown carbon, *Chem. Rev.*, 2015, **115**, 4335–4382.

7 C. Li, Q. He, A. P. S. Hettiyadura, U. Käfer, G. Shmul, D. Meidan, R. Zimmermann, S. S. Brown, C. George, A. Laskin and Y. Rudich, Formation of Secondary Brown Carbon in Biomass Burning Aerosol Proxies through NO3 Radical Reactions, *Environ. Sci. Technol.*, 2020, **54**, 1395–1405.

8 Y. Kuang, B. Luo, S. Huang, J. Liu, W. Hu, Y. Peng, D. Chen, D. Yue, W. Xu, B. Yuan and M. Shao, Formation of highly absorptive secondary brown carbon through nighttime multiphase chemistry of biomass burning emissions, *Atmos. Chem. Phys.*, 2025, **25**, 3737–3752.

9 X. Wang, R. K. Chakrabarty, J. P. Schwarz, S. M. Murphy, E. J. Levin, S. G. Howell, H. Guo, P. Campuzano-Jost and J. L. Jimenez, Dark brown carbon from biomass burning contributes to significant global-scale positive forcing, *One Earth*, 2025, **8**, 101205.

© 2026 The Author(s). Published by the Royal Society of Chemistry

10 L. Ferrero, A. Riccio, M. G. Perrone, G. Sangiorgi, B. S. Ferrini and E. Bolzacchini, Mixing height determination by tethered balloon-based particle soundings and modeling simulations, *Atmos. Res.*, 2011, **102**, 145–156.
11 H. Diémoz, F. Barnaba, T. Magri, G. Pession, D. Dionisi, S. Pittavino, I. K. F. Tombolato, M. Campanelli, L. S. Della Ceca, M. Hervo, L. Di Liberto, L. Ferrero and G. P. Gobbi, Transport of Po Valley aerosol pollution to the northwestern Alps – Part 1: Phenomenology, *Atmos. Chem. Phys.*, 2019, **19**, 3065–3095.
12 F. Barnaba and G. P. Gobbi, Aerosol seasonal variability over the Mediterranean region and relative impact of maritime, continental and Saharan dust particles over the basin from MODIS data in the year 2001, *Atmos. Chem. Phys.*, 2004, **4**, 2367–2391.
13 W. Di Nicolantonio, A. Cacciari, E. Bolzacchini, L. Ferrero, M. Volta, and E. Pisoni, *MODIS Aerosol Optical Properties over North Italy for Estimating Surface-Level PM2.5, 2007*, Envisat Symposium, 2007.
14 W. Di Nicolantonio, A. Cacciari, A. Petritoli, C. Carnevale, E. Pisoni, M. L. Volta, P. Stocchi, G. Curci, E. Bolzacchini, L. Ferrero, C. Ananasso and C. Tomasi, MODIS and OMI satellite observations supporting air quality monitoring, *Radiat. Protect. Dosim.*, 2009, **137**, 280–287.
15 L. Ferrero, A. Riccio, B. S. Ferrini, L. D'Angelo, G. Rovelli, M. Casati, F. Angelini, F. Barnaba, G. P. Gobbi, M. Cataldi and E. Bolzacchini, Satellite AOD conversion into ground PM10, PM2.5 and PM1 over the Po valley (Milan, Italy) exploiting information on aerosol vertical profiles, chemistry, hygroscopicity and meteorology, *Atmos. Pollut. Res.*, 2019, **10**, 1895–1912.
16 Official Journal of the European Union, *DIRECTIVE (EU) 2016/2284 of the EUROPEAN PARLIAMENT and of the COUNCIL. Of 14 December 2016 on the Reduction of National Emissions of Certain Atmospheric Pollutants, Amending Directive 2003/35/EC and Repealing Directive 2001/8*, 2016.
17 Gazzetta Ufficiale della Repubblica Italiana, *Il Decreto-Legge 13 Giugno 2023, n. 69, Convertito Con la Legge 10 Agosto 2023, n. 103*, 2023.
18 J. David, L. D'Angelo, M. Simon and A. L. Vogel, Real-time organic aerosol characterization via Orbitrap mass spectrometry in urban and agricultural environments, *Atmos. Meas. Tech.*, 2025, **18**, 4573–4591.
19 ARPA Lombadia, *STAZIONE DI RILEVAMENTO*, https://www.arpalombardia.it/temi-ambientali/aria/stazioni-fisse/dettaglio-stazioni-fisse/?stazione=703, last accessed on 27 July 2026.
20 N. L. Ng, S. C. Herndon, A. Trimborn, M. R. Canagaratna, P. L. Croteau, T. B. Onasch, D. Sueper, D. R. Worsnop, Q. Zhang, Y. L. Sun and J. T. Jayne, An Aerosol Chemical Speciation Monitor (ACSM) for Routine Monitoring of the Composition and Mass Concentrations of Ambient Aerosol, *Aerosol Sci. Technol.*, 2011, **45**, 780–794.
21 C. Zuth, A. L. Vogel, S. Ockenfeld, R. Huesmann and T. Hoffmann, Ultrahigh-Resolution Mass Spectrometry in Real Time: Atmospheric Pressure Chemical Ionization Orbitrap Mass Spectrometry of Atmospheric Organic Aerosol, *Anal. Chem.*, 2018, **90**, 8816–8823.
22 T. Hoffmann, R. Bandur, U. Marggraf and M. Linscheid, Molecular composition of organic aerosols formed in the α-pinene/O 3 reaction: Implications for new particle formation processes, *J. Geophys. Res.*, 1998, **103**, 25569–25578.
23 U. Kückelmann, B. Warscheid and T. Hoffmann, On-line characterization of organic aerosols formed from biogenic precursors using atmospheric pressure chemical ionization mass spectrometry, *Anal. Chem.*, 2000, **72**, 1905–1912.
24 R. Cai, Y. Li, Y. Clément, D. Li, C. Dubois, M. Fabre, L. Besson, S. Perrier, C. George, M. Ehn, C. Huang, P. Yi, Y. Ma and M. Riva, Orbitool: a software tool for analyzing online Orbitrap mass spectrometry data, *Atmos. Meas. Tech.*, 2021, **14**, 2377–2387.
25 N. M. Donahue, A. L. Robinson, C. O. Stanier and S. N. Pandis, Coupled partitioning, dilution, and chemical aging of semivolatile organics, *Environ. Sci. Technol.*, 2006, **40**, 2635–2643.
26 N. M. Donahue, S. A. Epstein, S. N. Pandis and A. L. Robinson, A two-dimensional volatility basis set: 1. organic-aerosol mixing thermodynamics, *Atmos. Chem. Phys.*, 2011, **11**, 3303–3318.
27 Y. Li, U. Pöschl and M. Shiraiwa, Molecular corridors and parameterizations of volatility in the chemical evolution of organic aerosols, *Atmos. Chem. Phys.*, 2016, **16**, 3327–3344.
28 A. R. Koss, M. R. Canagaratna, A. Zaytsev, J. E. Krechmer, M. Breitenlechner, K. J. Nihill, C. Y. Lim, J. C. Rowe, J. R. Roscioli, F. N. Keutsch and J. H. Kroll, Dimensionality-reduction techniques for complex mass spectrometric datasets: application to laboratory atmospheric organic oxidation experiments, *Atmos. Chem. Phys.*, 2020, **20**, 1021–1041.
29 A. M. Middlebrook, R. Bahreini, J. L. Jimenez and M. R. Canagaratna, Evaluation of Composition-Dependent Collection Efficiencies for the Aerodyne Aerosol Mass Spectrometer using Field Data, *Aerosol Sci. Technol.*, 2012, **46**, 258–271.
30 M. Pitz, J. Cyrys, E. Karg, A. Wiedensohler, H. E. Wichmann and J. Heinrich, Variability of apparent particle density of an urban aerosol, *Environ. Sci. Technol.*, 2003, **37**, 4336–4342.
31 L. D'Angelo, G. Rovelli, M. Casati, G. Sangiorgi, M. G. Perrone, E. Bolzacchini and L. Ferrero, Seasonal behavior of PM2.5 deliquescence, crystallization, and hygroscopic growth in the Po Valley (Milan): Implications for remote sensing applications, *Atmos. Res.*, 2016, **176–177**, 87–95.
32 L. Drinovec, G. Močnik, P. Zotter, A. S. H. Prévôt, C. Ruckstuhl, E. Coz, M. Rupakheti, J. Sciare, T. Müller, A. Wiedensohler and A. D. A. Hansen, The "dual-spot" Aethalometer: an improved measurement of aerosol black carbon with real-time loading compensation, *Atmos. Meas. Tech.*, 2015, **8**, 1965–1979.
33 E. Weingartner, H. Saathoff, M. Schnaiter, N. Streit, B. Bitnar and U. Baltensperger, Absorption of light by soot particles:

 © 2026 The Author(s). Published by the Royal Society of Chemistry

determination of the absorption coefficient by means of aethalometers, *J. Aerosol Sci.*, 2003, **34**, 1445–1463.

34 M. Savadkoohi, M. Pandolfi, C. Reche, J. V. Niemi, D. Mooibroek, G. Titos, D. C. Green, A. H. Tremper, C. Hueglin, E. Liakakou, N. Mihalopoulos, I. Stavroulas, B. Artiñano, E. Coz, L. Alados-Arboledas, D. Beddows, V. Riffault, J. F. de Brito, S. Bastian, A. Baudic, C. Colombi, F. Costabile, B. Chazeau, N. Marchand, J. L. Gómez-Amo, V. Estellés, V. Matos, E. van der Gaag, G. Gille, K. Luoma, H. E. Manninen, M. Norman, S. Silvergren, J.-E. Petit, J.-P. Putaud, O. V. Rattigan, H. Timonen, T. Tuch, M. Merkel, K. Weinhold, S. Vratolis, J. Vasilescu, O. Favez, R. M. Harrison, P. Laj, A. Wiedensohler, P. K. Hopke, T. Petäjä, A. Alastuey and X. Querol, The variability of mass concentrations and source apportionment analysis of equivalent black carbon across urban Europe, *Environ. Int.*, 2023, **178**, 108081.

35 W. P. Arnott, K. Hamasha, H. Moosmüller, P. J. Sheridan and J. A. Ogren, Towards Aerosol Light-Absorption Measurements with a 7-Wavelength Aethalometer: Evaluation with a Photoacoustic Instrument and 3-Wavelength Nephelometer, *Aerosol Sci. Technol.*, 2005, **39**, 17–29.

36 O. Schmid, P. Artaxo, W. P. Arnott, D. Chand, L. V. Gatti, G. P. Frank, A. Hoffer, M. Schnaiter and M. O. Andreae, Spectral light absorption by ambient aerosols influenced by biomass burning in the Amazon Basin. I: Comparison and field calibration of absorption measurement techniques, *Atmos. Chem. Phys.*, 2006, **6**, 3443–3462.

37 J. Sandradewi, A. S. H. Prévôt, S. Szidat, N. Perron, M. R. Alfarra, V. A. Lanz, E. Weingartner and U. Baltensperger, Using aerosol light absorption measurements for the quantitative determination of wood burning and traffic emission contributions to particulate matter, *Environ. Sci. Technol.*, 2008, **42**, 3316–3323.

38 M. Collaud Coen, E. Weingartner, A. Apituley, D. Ceburnis, R. Fierz-Schmidhauser, H. Flentje, J. S. Henzing, S. G. Jennings, M. Moerman, A. Petzold, O. Schmid and U. Baltensperger, Minimizing light absorption measurement artifacts of the Aethalometer: evaluation of five correction algorithms, *Atmos. Meas. Tech.*, 2010, **3**, 457–474.

39 T. C. Bond, S. J. Doherty, D. W. Fahey, P. M. Forster, T. Berntsen, B. J. DeAngelo, M. G. Flanner, S. Ghan, B. Kärcher, D. Koch, S. Kinne, Y. Kondo, P. K. Quinn, M. C. Sarofim, M. G. Schultz, M. Schulz, C. Venkataraman, H. Zhang, S. Zhang, N. Bellouin, S. K. Guttikunda, P. K. Hopke, M. Z. Jacobson, J. W. Kaiser, Z. Klimont, U. Lohmann, J. P. Schwarz, D. Shindell, T. Storelvmo, S. G. Warren and C. S. Zender, Bounding the role of black carbon in the climate system: A scientific assessment, *J. Geophys. Res.*, 2013, **118**, 5380–5552.

40 H. Moosmüller, R. K. Chakrabarty and W. P. Arnott, Aerosol light absorption and its measurement: A review, *J. Quant. Spectrosc. Radiat. Transf.*, 2009, **110**, 844–878.

41 D. Baumgardner, O. Popovicheva, J. Allan, V. Bernardoni, J. Cao, F. Cavalli, J. Cozic, E. Diapouli, K. Eleftheriadis, P. J. Genberg, C. Gonzalez, M. Gysel, A. John, T. W. Kirchstetter, T. A. J. Kuhlbusch, M. Laborde, D. Lack, T. Müller, R. Niessner, A. Petzold, A. Piazzalunga, J. P. Putaud, J. Schwarz, P. Sheridan, R. Subramanian, E. Swietlicki, G. Valli, R. Vecchi and M. Viana, Soot reference materials for instrument calibration and intercomparisons: a workshop summary with recommendations, *Atmos. Meas. Tech.*, 2012, **5**, 1869–1887.

42 D. Massabò, L. Caponi, V. Bernardoni, M. C. Bove, P. Brotto, G. Calzolai, F. Cassola, M. Chiari, M. E. Fedi, P. Fermo, M. Giannoni, F. Lucarelli, S. Nava, A. Piazzalunga, G. Valli, R. Vecchi and P. Prati, Multi-wavelength optical determination of black and brown carbon in atmospheric aerosols, *Atmos. Environ.*, 2015, **108**, 1–12.

43 V. Moschos, C. Christensen, M. Mouton, M. N. Fiddler, T. Isolabella, F. Mazzei, D. Massabò, B. J. Turpin, S. Bililign and J. D. Surratt, Quantifying the Light-Absorption Properties and Molecular Composition of Brown Carbon Aerosol from Sub-Saharan African Biomass Combustion, *Environ. Sci. Technol.*, 2024, **58**, 4268–4280.

44 T. Müller, M. Fiebig, *ACTRIS in Situ Aerosol: Guidelines for Manual QC of AE33 Absorption Photometer Data*, 2018.

45 J. Yus-Díez, V. Bernardoni, G. Močnik, A. Alastuey, D. Ciniglia, M. Ivančič, X. Querol, N. Perez, C. Reche, M. Rigler, R. Vecchi, S. Valentini and M. Pandolfi, *Determination of the Multiple-Scattering Correction Factor and Its Cross-Sensitivity to Scattering and Wavelength Dependence for Different AE33 Aethalometer Filter Tapes: A Multi-instrumental Approach*, 2021.

46 L. Ferrero, V. Bernardoni, L. Santagostini, S. Cogliati, F. Soldan, S. Valentini, D. Massabò, G. Močnik, A. Gregorič, M. Rigler, P. Prati, A. Bigogno, N. Losi, G. Valli, R. Vecchi and E. Bolzacchini, Consistent determination of the heating rate of light-absorbing aerosol using wavelength- and time-dependent Aethalometer multiple-scattering correction, *Sci. Total Environ.*, 2021, **791**, 148277.

47 V. Moschos, M. Gysel-Beer, R. L. Modini, J. C. Corbin, D. Massabò, C. Costa, S. G. Danelli, A. Vlachou, K. R. Daellenbach, S. Szidat, P. Prati, A. S. H. Prévôt, U. Baltensperger and I. El Haddad, Source-specific light absorption by carbonaceous components in the complex aerosol matrix from yearly filter-based measurements, *Atmos. Chem. Phys.*, 2021, **21**, 12809–12833.

48 K. N. Liou, *An Introduction to Atmospheric Radiation*, Elsevier, 2002.

49 L. Ferrero, N. Losi, M. Rigler, A. Gregorič, C. Colombi, L. D'Angelo, E. Cuccia, A. M. Cefalì, I. Gini, A. Doldi, S. Cerri, P. Maroni, D. Cipriano, P. Markuszewski and E. Bolzacchini, Determining the Aethalometer multiple scattering enhancement factor C from the filter loading parameter, *Sci. Total Environ.*, 2024, **917**, 170221.

50 P. Tian, D. Liu, D. Zhao, C. Yu, Q. Liu, M. Huang, Z. Deng, L. Ran, Y. Wu, S. Ding, K. Hu, G. Zhao, C. Zhao and D. Ding, *In-situ Vertical Characteristics of Optical Properties and Heating Rates of Aerosol over Beijing*, 2019.

© 2026 The Author(s). Published by the Royal Society of Chemistry

51 V. Bernardoni, L. Ferrero, E. Bolzacchini, A. C. Forello, A. Gregorič, D. Massabò, G. Močnik, P. Prati, M. Rigler, L. Santagostini, F. Soldan, S. Valentini, G. Valli and R. Vecchi, Determination of Aethalometer multiple-scattering enhancement parameters and impact on source apportionment during the winter 2017/18 EMEP/ACTRIS/COLOSSAL campaign in Milan, *Atmos. Meas. Tech.*, 2021, **14**, 2919–2940.

52 V. Bernardoni, G. Valli and R. Vecchi, Set-up of a multi wavelength polar photometer for off-line absorption coefficient measurements on 1-h resolved aerosol samples, *J. Aerosol Sci.*, 2017, **107**, 84–93.

53 M. Ivančič, A. Gregorič, G. Lavrič, B. Alföldy, I. Ježek, S. Hasheminassab, P. Pakbin, F. Ahangar, M. Sowlat, S. Boddeker and M. Rigler, Two-year-long high-time-resolution apportionment of primary and secondary carbonaceous aerosols in the Los Angeles Basin using an advanced total carbon-black carbon (TC-BC(λ)) method, *Sci. Total Environ.*, 2022, **848**, 157606.

54 J. Schneider, S. Weimer, F. Drewnick, S. Borrmann, G. Helas, P. Gwaze, O. Schmid, M. O. Andreae and U. Kirchner, Mass spectrometric analysis and aerodynamic properties of various types of combustion-related aerosol particles, *Int. J. Mass Spectrom.*, 2006, **258**, 37–49.

55 N. L. Ng, M. R. Canagaratna, J. L. Jimenez, P. S. Chhabra, J. H. Seinfeld and D. R. Worsnop, Changes in organic aerosol composition with aging inferred from aerosol mass spectra, *Atmos. Chem. Phys.*, 2011, **11**, 6465–6474.

56 J. H. Kroll, N. M. Donahue, J. L. Jimenez, S. H. Kessler, M. R. Canagaratna, K. R. Wilson, K. E. Altieri, L. R. Mazzoleni, A. S. Wozniak, H. Bluhm, E. R. Mysak, J. D. Smith, C. E. Kolb and D. R. Worsnop, Carbon oxidation state as a metric for describing the chemistry of atmospheric organic aerosol, *Nat. Chem.*, 2011, **3**, 133–139.

57 A. C. Aiken, P. F. Decarlo, J. H. Kroll, D. R. Worsnop, J. A. Huffman, K. S. Docherty, I. M. Ulbrich, C. Mohr, J. R. Kimmel, D. Sueper, Y. Sun, Q. Zhang, A. Trimborn, M. Northway, P. J. Ziemann, M. R. Canagaratna, T. B. Onasch, M. R. Alfarra, A. S. H. Prevot, J. Dommen, J. Duplissy, A. Metzger, U. Baltensperger and J. L. Jimenez, O/C and OM/OC ratios of primary, secondary, and ambient organic aerosols with high-resolution time-of-flight aerosol mass spectrometry, *Environ. Sci. Technol.*, 2008, **42**, 4478–4485.

58 B. R. Simoneit, Biomass burning — a review of organic tracers for smoke from incomplete combustion, *Appl. Geochem.*, 2002, **17**, 129–162.

59 R. L. Evans, D. J. Bryant, A. Voliotis, D. Hu, H. Wu, S. A. Syafira, O. E. Oghama, G. McFiggans, J. F. Hamilton and A. R. Rickard, *The Importance of Burning Conditions on the Composition of Domestic Biomass Burning Organic Aerosol and the Impact of Atmospheric Aging*, 2024.

60 P. E. Kolattukudy, Biopolyester membranes of plants: cutin and suberin, *Science*, 1980, **208**, 990–1000.

61 W. F. Rogge, L. M. Hildemann, M. A. Mazurek, G. R. Cass and B. R. T. Simoneit, Sources of Fine Organic Aerosol. 9. Pine, Oak, and Synthetic Log Combustion in Residential Fireplaces, *Environ. Sci. Technol.*, 1998, **32**, 13–22.

62 M. He and N.-Z. Ding, Plant Unsaturated Fatty Acids: Multiple Roles in Stress Response, *Front. Plant Sci.*, 2020, **11**, 562785.

63 A. Yazdani, S. Takahama, J. K. Kodros, M. Paglione, M. Masiol, S. Squizzato, K. Florou, C. Kaltsonoudis, S. D. Jorga, S. N. Pandis and A. Nenes, Chemical evolution of primary and secondary biomass burning aerosols during daytime and nighttime, *Atmos. Chem. Phys.*, 2023, **23**, 7461–7477.

64 E. Kostenidou, E. Karnezi, A. Kolodziejczyk, R. Szmigielski and S. N. Pandis, Physical and Chemical Properties of 3-Methyl-1,2,3-butanetricarboxylic Acid (MBTCA) Aerosol, *Environ. Sci. Technol.*, 2018, **52**, 1150–1155.

65 K. Kristensen, T. Cui, H. Zhang, A. Gold, M. Glasius and J. D. Surratt, Dimers in α-pinene secondary organic aerosol: effect of hydroxyl radical, ozone, relative humidity and aerosol acidity, *Atmos. Chem. Phys.*, 2014, **14**, 4201–4218.

66 Y. Guo, C. Yan, Y. Liu, X. Qiao, F. Zheng, Y. Zhang, Y. Zhou, C. Li, X. Fan, Z. Lin, Z. Feng, Y. Zhang, P. Zheng, L. Tian, W. Nie, Z. Wang, D. Huang, K. R. Daellenbach, L. Yao, L. Dada, F. Bianchi, J. Jiang, Y. Liu, V.-M. Kerminen and M. Kulmala, Seasonal variation in oxygenated organic molecules in urban Beijing and their contribution to secondary organic aerosol, *Atmos. Chem. Phys.*, 2022, **22**, 10077–10097.

67 Q. He, S. Tomaz, C. Li, M. Zhu, D. Meidan, M. Riva, A. Laskin, S. S. Brown, C. George, X. Wang and Y. Rudich, Optical Properties of Secondary Organic Aerosol Produced by Nitrate Radical Oxidation of Biogenic Volatile Organic Compounds, *Environ. Sci. Technol.*, 2021, **55**, 2878–2889.

68 L. T. Fleming, P. Lin, A. Laskin, J. Laskin, R. Weltman, R. D. Edwards, N. K. Arora, A. Yadav, S. Meinardi, D. R. Blake, A. Pillarisetti, K. R. Smith and S. A. Nizkorodov, Molecular composition of particulate matter emissions from dung and brushwood burning household cookstoves in Haryana, India, *Atmos. Chem. Phys.*, 2018, **18**, 2461–2480.

69 J. S. Smith, A. Laskin and J. Laskin, Molecular characterization of biomass burning aerosols using high-resolution mass spectrometry, *Anal. Chem.*, 2009, **81**, 1512–1521.

70 D. C. Carslaw, J. Davison and K. Ropkins, *CRAN: Contributed Packages*, 2010.

71 D. C. Carslaw and K. Ropkins, openair — An R package for air quality data analysis, *Environ. Model. Software*, 2012, **27–28**, 52–61.

72 J. Song, M. Li, C. Zou, T. Cao, X. Fan, B. Jiang, Z. Yu, W. Jia and P. Peng, Molecular Characterization of Nitrogen-Containing Compounds in Humic-like Substances Emitted from Biomass Burning and Coal Combustion, *Environ. Sci. Technol.*, 2022, **56**, 119–130.

73 Z. Safaei, A. Shiroudi, E. Zahedi and M. Sillanpää, Atmospheric oxidation reactions of imidazole initiated by hydroxyl radicals: kinetics and mechanism of reactions

 © 2026 The Author(s). Published by the Royal Society of Chemistry

and atmospheric implications, *Phys. Chem. Chem. Phys.*, 2019, **21**, 8445–8456.
74 L. Li, Y. Han, J. Li, Y. Lin, X. Zhang, Q. Wang and J. Cao, Effects of photochemical aging on the molecular composition of organic aerosols derived from agricultural biomass burning in whole combustion process, *Sci. Total Environ.*, 2024, **946**, 174152.
75 D. Hoffmann, A. Tilgner, Y. Iinuma and H. Herrmann, Atmospheric Stability of Levoglucosan: A Detailed Laboratory and Modeling Study, *Environ. Sci. Technol.*, 2010, **44**, 694–699.
76 C. Lai, Y. Liu, J. Ma, Q. Ma and H. He, Degradation kinetics of levoglucosan initiated by hydroxyl radical under different environmental conditions, *Atmos. Environ.*, 2014, **91**, 32–39.
77 H. Bhattarai, E. Saikawa, X. Wan, H. Zhu, K. Ram, S. Gao, S. Kang, Q. Zhang, Y. Zhang, G. Wu, X. Wang, K. Kawamura, P. Fu and Z. Cong, Levoglucosan as a tracer of biomass burning: Recent progress and perspectives, *Atmos. Res.*, 2019, **220**, 20–33.
78 G. Schkolnik and Y. Rudich, Detection and quantification of levoglucosan in atmospheric aerosols: a review, *Anal. Bioanal. Chem.*, 2006, **385**, 26–33.
79 J. Bai, X. Sun, C. Zhang, Y. Xu and C. Qi, The OH-initiated atmospheric reaction mechanism and kinetics for levoglucosan emitted in biomass burning, *Chemosphere*, 2013, **93**, 2004–2010.
80 Y. Sun, L. Liu, M. Li, X. Chen and F. Xu, Theoretical investigation on the mechanisms and kinetics of OH/NO3-initiated atmospheric oxidation of vanillin and vanillic acid, *Chemosphere*, 2022, **288**, 132544.
81 R. Atkinson, Kinetics and Mechanisms of the Gas-Phase Reactions of the NO3 Radical with Organic Compounds, *J. Phys. Chem. Ref. Data*, 1991, **20**, 459–507.
82 N. Xu, M. Hu, X. Li, L. Zeng, Y. Wang, Y. Qiu, K. Song, S. Li, S. Shuai, Y. Chen, J. Hu and S. Guo, Unraveling the Light-Absorbing Properties of Brown Carbon at a Molecular Level, *Geophys. Res. Lett.*, 2024, **51**, e2024GL108834.
83 V. Gold and A. McNaught, eds., *The IUPAC Compendium of Chemical Terminology*, International Union of Pure and Applied Chemistry (IUPAC), Research Triangle Park, NC, 2025.
84 P. Lin, L. T. Fleming, S. A. Nizkorodov, J. Laskin and A. Laskin, Comprehensive Molecular Characterization of Atmospheric Brown Carbon by High Resolution Mass Spectrometry with Electrospray and Atmospheric Pressure Photoionization, *Anal. Chem.*, 2018, **90**, 12493–12502.
85 J. Zhai, Y. Zhang, P. Liu, Y. Zhang, A. Zhang, Y. Zeng, B. Cai, J. Zhang, C. Xing, H. Yang, X. Wang, J. Ye, C. Wang, T.-M. Fu, L. Zhu, H. Shen, S. Tao and X. Yang, Source-dependent optical properties and molecular characteristics of atmospheric brown carbon, *Atmos. Chem. Phys.*, 2025, **25**, 7959–7972.
86 R. Saleh, From Measurements to Models: Toward Accurate Representation of Brown Carbon in Climate Calculations, *Curr. Pollut. Rep.*, 2020, **6**, 90–104.

© 2026 The Author(s). Published by the Royal Society of Chemistry